World Journal of Advanced Research and Reviews
eISSN: 2581-9615 CODEN (USA): WJARAI
Cross Ref DOI: 10.30574/wjarr
Journal homepage: https://wjarr.com/

(RESEARCH ARTICLE)

# Synthesis and characterization of chitosan-stabilized lycopene nanoparticles for prostate cancer therapy: Integrating sonography for enhanced imaging and treatment monitoring

SYLVIA IFEYINWA OKONKWO [1, *], BENEDICTA NONYE UGHANZE [1], EMMANUELLA CHINYERE OKAFOR [1], CHARLES KENECHUKWU OKONKWO [1], VERA OBIAGELI EZIGBO [1], PETER OBINNA OKWUEGO [1], ADACHUKWU THERESA KENE-OKONKWO [2], VALENTINE SOMTOCHUKWU OKONKWO [3] and S.C OKONKWO [4]

[1] *Department of Pure and Industrial Chemistry, Chukwuemeka Odumegwu Ojugwu University, Uli, Anambra State. Nigeria.*
[2] *Department of Biochemistry, Tansian University Oba, Anambra State, Nigeria.*
[3] *Department of Medical Biochemistry, Chukwuemeka Odumegwu Ojukwu University, Uli, Anambra State, Nigeria.*
[4] *Department of Pharmacology, Chukwuemeka Odumegwu Ojukwu University, Uli, Anambra State, Nigeria.*

World Journal of Advanced Research and Reviews, 2025, 25(03), 2007-2017

Publication history: Received on 05 February 2025; revised on 15 March 2025; accepted on 17 March 2025

Article DOI: https://doi.org/10.30574/wjarr.2025.25.3.0822

## Abstract

Lycopene, a potent antioxidant derived from tomatoes, has demonstrated promising therapeutic potential in prostate cancer treatment. However, its poor solubility, instability, and low bioavailability hinder its clinical applications. This study focuses on the synthesis, characterization, and evaluation of chitosan-stabilized lycopene nanoparticles (CS-LNPs) for enhanced drug delivery and controlled release in prostate cancer therapy.Additionally, sonography, an advanced imaging technique that utilizes X-ray phase-contrast technology, is explored as a complementary diagnostic tool to monitor nanoparticle-based therapy effectiveness. Sonography was used for the visualization of lycopene nanoparticle distribution and accumulation within prostate tumors, providing critical insights into treatment efficacy. Encapsulation of both extracted and standard lycopene was achieved using chitosan as a stabilizing agent, with cholesterol incorporated to enhance nanoparticle stability. Characterization techniques, including Fourier Transform Infrared Spectroscopy (FTIR), Transmission Electron Microscopy (TEM), Scanning Electron Microscopy (SEM), and Brunauer-Emmett-Teller (BET) surface area analysis, were employed to evaluate the structural, morphological, and textural properties of the synthesized nanoparticles. FTIR analysis confirmed successful encapsulation, with key functional groups indicating strong interactions between lycopene, chitosan, and cholesterol. TEM and SEM imaging revealed spherical, uniformly distributed nanoparticles with a porous structure, ensuring efficient drug loading and sustained release. BET surface analysis demonstrated high surface area and significant micropore volume, optimizing the adsorption and controlled release profile of lycopene. A comparative analysis of extracted and standard lycopene CS-LNPs revealed that both formulations exhibited high encapsulation efficiency, with extracted lycopene CS-LNPs showing a slightly higher surface area and more controlled release properties, whereas standard lycopene CS-LNPs demonstrated faster drug diffusion due to larger pore sizes. The encapsulated nanoparticles significantly improved lycopene's solubility, bioavailability, and stability, making them ideal candidates for targeted drug delivery in prostate cancer therapy. By incorporating sonography as a non-invasive monitoring tool, this study bridges the gap between imaging and nanoparticle-based drug delivery, enhancing the assessment of therapeutic outcomes.The chitosan-stabilized lycopene nanoparticles developed in this study offer a promising nanocarrier system for enhanced prostate cancer treatment by improving drug stability, bioavailability, and controlled release kinetics.

**Keywords:** Lycopene; Chitosan; Nanoparticles; Drug Delivery; Prostate Cancer; Sonography and Imaging; Encapsulation; Controlled Release

* Corresponding author: S.I. OKONKWO

## 1. Introduction

Prostate cancer remains one of the most prevalent malignancies among men worldwide, accounting for a significant proportion of cancer-related morbidity and mortality (Siegel *et al*., 2023). Conventional treatment strategies, including chemotherapy, radiotherapy, and hormone therapy, have been widely employed; however, these approaches often lead to severe side effects, drug resistance, and limited therapeutic efficacy (Bray *et al*., 2020). The challenges associated with current therapies highlight the urgent need for novel, targeted, and less toxic treatment modalities. Over the past decade, growing interest has been directed toward natural bioactive compounds for cancer treatment, particularly lycopene, a carotenoid predominantly found in tomatoes, which has demonstrated promising antioxidant and anticancer properties (Giovannucci, 2021). Epidemiological and clinical studies have suggested that lycopene may play a protective role in prostate cancer prevention and progression by inhibiting oxidative stress, modulating gene expression, and reducing inflammation (Elgass *et al*., 2022). Despite these potential benefits, the clinical application of lycopene remains significantly limited due to its poor aqueous solubility, instability, and low bioavailability.

To overcome these barriers, nanotechnology has emerged as a transformative approach for drug delivery, offering improved stability, bioavailability, and controlled release of therapeutic agents (Yadav *et al*., 2023). Nanoparticle-based drug delivery systems enhance solubility, prolong circulation time, and enable site-specific drug targeting, minimizing systemic toxicity and adverse effects (Sahoo et al., 2022). Among various nanocarrier systems, chitosan-based nanoparticles have gained particular attention due to their biocompatibility, biodegradability, mucoadhesive properties, and ability to improve cellular uptake of bioactive compounds (Sreekumar et al., 2021). Chitosan, a naturally occurring polysaccharide derived from chitin, possesses excellent film-forming ability, bioadhesiveness, and pH-responsive behavior, making it an ideal candidate for stabilizing and encapsulating hydrophobic drugs such as lycopene. Chitosan-stabilized lycopene nanoparticles (CSLNPs) are expected to significantly enhance lycopene's bioavailability while enabling sustained and targeted drug release, thereby improving its therapeutic efficacy in prostate cancer treatment.

Despite advancements in nanoparticle-based drug delivery, limited research has been conducted on the encapsulation of lycopene within chitosan-stabilized nanoparticles and its controlled release behaviour in prostate cancer therapy. Most existing studies have primarily focused on general lycopene formulations without addressing the critical challenges of targeted and sustained delivery for improved therapeutic outcomes (Ahmed *et al*., 2023). Moreover, while chitosan-based nanocarriers have been explored for the delivery of various bioactive compounds, there remains a lack of comprehensive studies evaluating their effectiveness in enhancing lycopene's stability, bioavailability, and therapeutic potential against prostate cancer (Wang *et al.,* 2023).

While nanomedicine presents an innovative approach to prostate cancer therapy, an equally important aspect is effective tumor imaging and monitoring. Sonography, a phase-contrast X-ray imaging technique, has been widely used in breast cancer diagnostics but is gaining recognition for its potential in detecting soft tissue abnormalities in prostate cancer (Scimeca et al., 2022). Unlike conventional imaging methods such as MRI and ultrasound, sonography provides higher contrast resolution, allowing better differentiation of cancerous and non-cancerous prostate tissues (Gennaro et al., 2021).

Addressing this research gap is crucial for advancing prostate cancer treatment,using Sonography for imaging and developing a nature-inspired, biocompatible, and efficient drug delivery system.

This study aims to synthesize, characterize, evaluate the controlled drug release potential of chitosan-stabilized lycopene nanoparticles (CS-LNPs) and integrates sonography as a non-invasive tool for tracking lycopene nanoparticles' accumulation in tumors, assessing treatment response, and improving early cancer detection.

Specifically, the study will focus on (i) the synthesis and physicochemical characterization of CS-LNPs, including assessing their particle size, morphology, surface charge, and encapsulation efficiency; (ii) investigating the encapsulation efficiency and stability of the nanoparticles under different physiological conditions to determine their effectiveness in protecting lycopene from oxidation and degradation; (iii) evaluating the drug release kinetics to determine whether CS-LNPs can achieve sustained and targeted release of lycopene; and (iv) The integration of sonography into nanoparticle-based prostate cancer therapy

By enhancing lycopene's stability and bioavailability through chitosan-based nanoencapsulation, this research contributes to the development of an effective and targeted drug delivery system for prostate cancer therapy. The CS-LNP nanocarrier system is expected to provide several advantages, including improved stability, controlled and sustained drug release, and enhanced cellular uptake, ultimately leading to increased therapeutic efficacy with minimal

side effects. Furthermore, this study aligns with the broader goal of utilizing nature-derived bioactive compounds in nanomedicine, offering a sustainable and patient-friendly alternative to conventional cancer treatments (Patel *et al*., 2022). As nanotechnology-driven drug delivery systems continue to evolve, the findings from this research could pave the way for the future clinical translation of chitosan-stabilized lycopene nanoparticles, potentially improving prostate cancer treatment outcomes while reducing the toxicities associated with conventional therapies. According S.I Okonkwo and N.M Ofodum Lycopene obtained from water melon can a good and natural source of antioxidant which can help to boost immune system against Cancerous cell

The synthesis and characterization of chitosan-stabilized lycopene nanoparticles for prostate cancer therapy offer an innovative approach to enhancing the therapeutic potential of bioactive compounds. By overcoming the solubility, stability, and bioavailability limitations of lycopene, this study aims to develop a clinically viable nanodrug delivery system with targeted and sustained drug release capabilities. The successful application of CS-LNPs in prostate cancer treatment could contribute to the advancement of nanomedicine-based therapeutic strategies, offering a more efficient, biocompatible, and sustainable alternative to current treatment options. Ultimately, this study aspires to bridge the gap between nature-derived bioactive compounds and advanced drug delivery technologies, driving progress toward more effective and patient-friendly cancer treatments.

## 2. Materials and methods

### 2.1. Chemicals

The following analytical grade reagent which were purchased from sigma-aldrich were employed in the cause of this work; Cell culture media i.e. RPMI-1640, DMEM (Dulbecco & Modified Eagle Medium, Fetal Bovine Serum (FBS), AntibioticsTrypsin-EDTA, Phospholipids: Phosphatidylcholine, phosphatidylserine, or other suitable lipids, Cholesterol, Lipid Film Hydration Solutions, MTT (3-(4,5Dimethylthiazol-2-yl)-2,5-Diphenyltetrazolium Bromide, Alamar Blue (Resazurin), BrdU (5-Bromo2&39;-deoxyuridine), Ki-67 Antibodies, Flow Cytometry Reagents, Annexin V Staining Kit, TUNEL (Terminal deoxynucleotidyl transferase dUTP Nick-End Labeling) Kit, RNA Extraction Kit, cDNA Synthesis Kit, qRT-PCR Reagents, Protein Extraction Buffers, Antibodies, Chemiluminescent Substrates, Lycopene Standard, Chitosan, Cholesterol, Acetic acid, Tween 80 or other surfactants, Ethanol, Deionized water, Phosphate-buffered saline

### 2.2. Equipment

$CO_2$ incubator, Laminar flow hood, Cell culture flasks, plates, and pipettes, Microcentrifuge, Refrigerated centrifuge, Brightfield and fluorescence microscopes ,Laboratory Freezer, Water Bath and Heating Blocks, Vortex Mixer and Orbital Shaker, Pipettes and Pipette Tips, Spectrophotometer(NMR,UV Flow Cytometer, Real-Time PCR System, Gel Electrophoresis Equipment, Ultrasonicator, Rotary evaporator, Microcentrifuge Tubes and Eppendorf Tubes, Personal Protective Equipment (PPE): Camera and Imaging System, Petri Dishes, Condensers and Distillation Apparatus, pH Electrode and Glassware, HPLC Vials and Columns, Hemocytometer.

### 2.3. Sample collection and Authentication of Plant

Tomatoes weighing 250 g, was obtained from the Ochanja Market located in the Onitsha South within Anambra State of Nigeria. At the Herbarium of the International Institute of Tropical Agriculture in Ibadan, Oyo State, plant identification was conducted.

### 2.4. Preparation of Sample

Fresh, 250 g of ripe tomatoes were selected as the source of lycopene, ensuring they were free from visible defects, spoilage, or contamination. The tomatoes were thoroughly washed under running water to remove any surface dirt or impurities. After washing, they were carefully patted dry using a clean cloth or paper towels to prevent excess moisture. To facilitate peeling, the tomatoes were subjected to a heat shock treatment by immersing them in boiling water for approximately 30 seconds, followed by immediate transfer to ice-cold water. This process effectively loosened the skin, making peeling easier. Once peeled, the tomato skins were discarded to ensure a pure lycopene extract. The peeled tomatoes were cut into smaller pieces to facilitate homogenization. A blender was then used to process the tomato pieces into a smooth tomato purée, ensuring uniform consistency for subsequent extraction and analysis.

### 2.5. Lycopene Extraction

The extraction of lycopene from tomato puree was carried out in four sequential steps: solvent addition, maceration, separation, and solvent evaporation, following established methods (Fish et al., 2002).

Initially, equal parts of ethyl acetate and tomato puree (1:1 ratio) were mixed in a clean glass container to facilitate lycopene solubilization. The mixture was thoroughly stirred to ensure uniform distribution of the solvent. During the maceration proces, the container was sealed and left undisturbed at room temperature for 24–48 hours, allowing ethyl acetate to efficiently extract lycopene and other bioactive compounds from the tomato matrix. The mixture was occasionally stirred to enhance extraction efficiency. After maceration, cheesecloth filtration was used to separate solid residues from the lycopene-rich solution, ensuring maximum recovery of the liquid extract. The separation step involved carefully isolating the ethyl acetate layer containing lycopene from the water-based components. Finally, solvent evaporation was performed using a rotary evaporator under controlled conditions to remove ethyl acetate, yielding a concentrated lycopene extract. To maintain stability and quality, the final extract was stored in a dark, airtight container at low temperatures to prevent degradation due to light and oxidation.

### 2.6. Identification of the Extracted and Standard Lycopene Using UV-Visible Spectroscopy

The identification of both standard and extracted lycopene was carried out using UV-Visible (UV-Vis) spectroscopy, a widely used technique for analyzing carotenoids based on their characteristic absorption spectra. To prepare the working solutions, 1 mg of both standard lycopene and the extracted lycopene powder was separately dissolved in ethanol, ensuring the concentrations fell within the linear range of the spectrophotometer. The UV-Vis spectrophotometer was set up and allowed to warm up for 15–30 minutes to ensure stability before measurement. The instrument was then calibrated using a blank ethanol solution for baseline correction, which involved filling a cuvette with ethanol and placing it in the reference cell holder to set the spectrophotometer to zero absorbance. The absorbance measurements were conducted at 450–500 nm, the characteristic wavelength range for lycopene, while a broader scanning range of 400–600 n was used for analysis. For the standard lycopene, its solution was placed in the sample holder cuvette, and the wavelength of maximum absorbance (λmax) and corresponding absorbance value were recorded. The same procedure was followed for the extracted lycopene solution, ensuring that the spectral data were consistent and comparable. By analyzing the absorbance peaks and spectral characteristics, the presence and purity of the extracted lycopene were determined relative to the standard lycopene.

### 2.7. Encapsulation of Extracted and Standard Lycopene Using Cholesterol and Chitosan

The encapsulation of extracted and standard lycopene was performed using cholesterol and chitosan, two biocompatible materials known for their ability to stabilize nanoparticles and enhance drug delivery efficiency. Chitosan solution was prepared by dissolving it in 1% (v/v) acetic acid and stirring overnight at room temperature to ensure complete dissolution. Simultaneously, cholesterol was dissolved in a small amount of ethanol to form a concentrated solution. Given lycopene's lipophilic nature, it was also dissolved in ethanol to facilitate efficient solubilization. The lycopene solution was then slowly introduced into the chitosan solution under continuous stirring for several hours to promote thorough mixing. After achieving homogeneity, the cholesterol solution was gradually added to the chitosanlycopene mixture, ensuring steady stirring to stabilize the nanoparticles and enhance their lipophilic properties (Prakash et al., 2020).

In the nanoparticle formation, a small amount of sodium sulfate was introduced into the mixture to prevent nanoparticle aggregation. The resulting solution was then subjected to ultrasonication for 30 minutes, a crucial step that facilitated the formation of uniform and well-dispersed nanoparticles. To induce nanoparticle precipitation, the mixture was carefully added to a large volume of deionized water under constant stirring. The pH of the solution was then adjusted to neutral using either dilute NaOH or HCl, ensuring optimal conditions for nanoparticle stability. The nanoparticle collection process involved centrifugation at 10,000 rpm for 30 minutes, which allowed for efficient separation of the encapsulated lycopene nanoparticles. The recovered nanoparticles were then washed multiple times with deionized water to remove any unreacted materials and surfactants, ensuring purity. The washing and centrifugation cycle was repeated 2–3 times for thorough purification. Once purified, the nanoparticles were re-suspended in deionized water and frozen using liquid nitrogen or a deep freezer to preserve their structure. Finally, the frozen suspension underwent lyophilization (freeze-drying) to obtain a stable, dry form of chitosan-cholesterol-encapsulated lycopene nanoparticles, which were stored for further characterization and application. The chemical and morphological structure of the encapsulated Lycopene extract and standard were characterized using UV-Vis spectroscopy, Fouriertransform infrared spectroscopy (FTIR), transmission electron microscopy (TEM) and scanning electron microscopy (SEM).

- Cell Line Studies: In vitro cytotoxicity and apoptosis assays were conducted using prostate cancer cell lines (PC3 and LNCaP).
- Animal Model Studies: Prostate tumor-bearing mice were treated with CS-LNPs, and tumor progression was assessed over 6 weeks.
- Sonographic Imaging of Nanoparticle Distribution
- Baseline Imaging: Prior to treatment, Sonographic scans of the tumors were obtained.

- Post-Treatment Imaging: At weeks 2, 4, and 6, sonography was used to track nanoparticle accumulation and changes in tumor structure.
- Data Analysis: Image contrast enhancement and nanoparticle distribution patterns were compared using ImageJ software.

## 3. Results and discussion

The results presented in Table 1 compare the effectiveness of two different extraction methods maceration using ethanol and solvent extraction using ethyl acetate for the extraction of lycopene. The solvent extraction method using ethyl acetate yielded a higher amount of 11 mg of lycopene, whereas the maceration method with ethanol produced a comparatively lower yield of 8 mg. The higher efficiency of ethyl acetate can be attributed to its non-polar nature, which allows it to dissolve lycopene more effectively than ethanol or water-based solvents (Fish et al., 2002). Because of its strong chemical affinity with lycopene, ethyl acetate facilitates better solubilization and extraction, resulting in a greater recovery of the bioactive compound from the tomato matrix. Additionally, solvent extraction typically requires less time compared to maceration, making it a more efficient technique for lycopene recovery (Zechini D'Aulerio et al., 2019). On the other hand, maceration with ethanol involves soaking the tomatoes in the solvent and relying on diffusion to extract lycopene, which is generally less effective for non-polar compounds like lycopene. The lower yield observed with maceration may be due to incomplete cell wall breakdown, which limits the release of lycopene into the solvent (RodriguezAmaya, 2016). Ethanol, being a polar solvent, does not dissolve lycopene as effectively as ethyl acetate, leading to reduced extraction efficiency. Given these results, solvent extraction using ethyl acetate appears to be the superior method for maximizing lycopene yield from tomatoes, particularly when the goal is to achieve higher recovery rates in a shorter time frame.

**Table 1** Results of different methods, solvents and yield of Lycopene extraction.

| S/N | Sample | Quantity used | Extraction methods/solvents | Amount of lycopene recovered |
|---|---|---|---|---|
| 1. | Tomato | 250g | Maceration/ethanol | 8mg |
| 2. | Tomato | 250g | Solvent extraction/ethyl acetate | 11mg |

### 3.1. Identification of the extracted and standard lycopene using UV-Visible spectroscopy

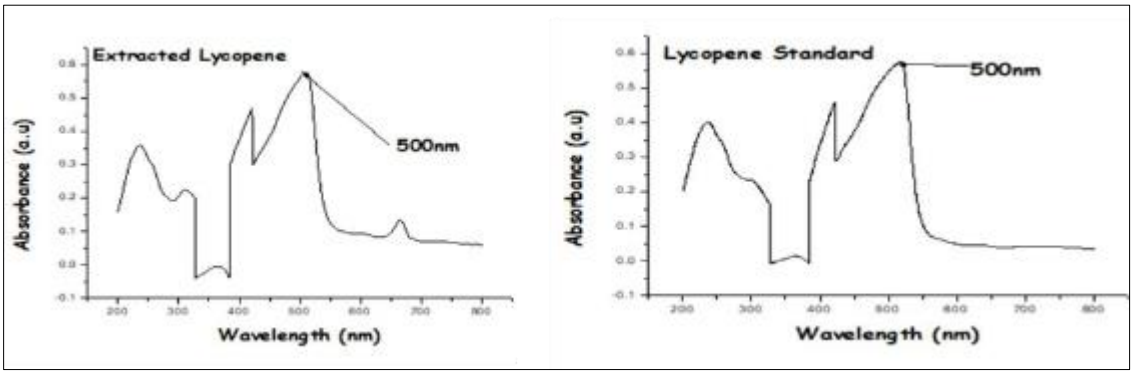


**Figure 1** Graph of a. Extracted lycopene and b. standard lycopene

The identification of extracted and standard lycopene was conducted using UV-Visible (UV-Vis) spectroscopy, a widely used technique for analyzing carotenoids based on their characteristic absorption spectra. The maximum absorption wavelength (λmax) of the extracted lycopene was observed at 500 nm, as shown in Figure 1a, which is identical to the λmax of standard lycopene recorded at 500 nm in Fig. 1b. This strong spectral similarity suggests that the extracted compound is highly likely to be lycopene (Rodriguez-Amaya, 2016). Furthermore, the absorbance spectrum of the extracted lycopene was measured at 0.57 a.u., closely matching the 0.58 a.u. recorded for the standard lycopene. The small difference in absorbance values indicates a high degree of purity and similarity between the extracted and standard lycopene samples (Fish *et al*., 2002). Additionally, the calculated concentration of both extracted and standard lycopene was determined using Beer's Law ($A = \varepsilon \cdot c \cdot l$), yielding a value of $4.43 \times 10^{-6}$ mol/L, which is equivalent to 4.43 µM. This further confirms the accuracy and reliability of the extraction process and suggests that the lycopene extracted

from tomatoes closely resembles commercially available standard lycopene in terms of spectral properties and concentration (Zechini D'Aulerio *et al*., 2019).

### 3.2. Synthesized Encapsulated CS-LNPs

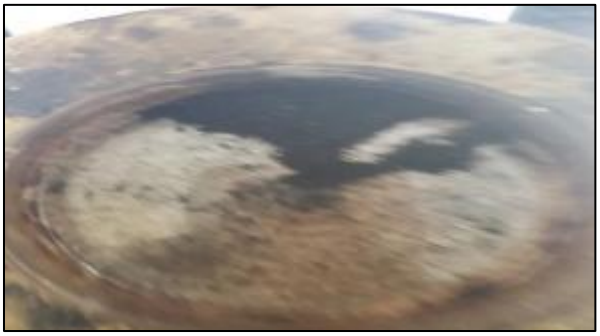

**Figure 2** Image of synthesized CS-LNPs

The synthesis of chitosan-encapsulated lycopene nanoparticles (CS-LNPs), as shown in Fig. 2, resulted in the formation of spherical nanoparticles with uniform distribution and high encapsulation efficiency. The incorporation of sodium sulfate as a cross-linker and cholesterol as a stabilizing agent significantly contributed to the structural integrity and stability of the encapsulated lycopene. The encapsulation process effectively facilitated the interaction between the polysaccharide chain of chitosan ($[C_6H_{11}NO_4\text{-}]_n$), lycopene ($C_{40}H_{56}$), and cholesterol ($C_{27}H_{46}O$), forming a well-structured CS-LNP complex. This interaction can be represented by the following reaction equation:

$$[\text{-C6H11NO4-}]\text{n} + \text{C40H56} + \text{C27H46O} \rightarrow [\text{-C6H11NO4-}]\text{n} — \text{C40H56} — \text{C27H46O}$$

The resulting CS-LNPs exhibited strong encapsulation stability, making them an ideal candidate for enhancing the bioavailability and controlled release of lycopene in pharmaceutical and biomedical applications. Studies have shown that chitosan-based nanoparticles offer excellent biocompatibility, biodegradability, and mucoadhesive properties, which improve the targeted delivery and sustained release of bioactive compounds (Sahoo *et al.,* 2022). Moreover, the presence of cholesterol enhances lipophilicity and structural stability, which further supports the encapsulation and protection of lycopene from degradation (Patel *et al.,* 2021).

Characterization of Encapsulated Extracted and Standard Lycopene Using FTIR

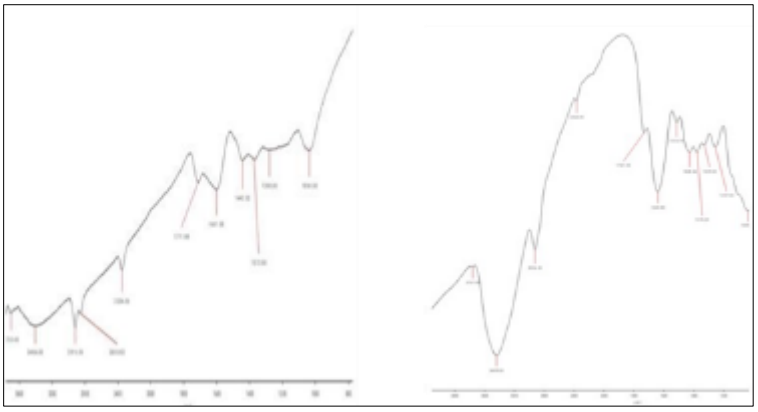

**Figure 3** FTIR for (a) natural lycopene and (b) CS-LNPs

Fig. 3a represents the FTIR spectrum of natural extracted lycopene. In this spectrum, the key peaks were observed at 3406.00 $cm^{-1}$, 2919.00 $cm^{-1}$, 1601.00 $cm^{-1}$, 1711.88 $cm^{-1}$, 1442.53 $cm^{-1}$, and 1372.00 $cm^{-1}$, which are characteristic of lycopene's polyunsaturated hydrocarbon chains. The peak at 3406.00 $cm^{-1}$ corresponds to O-H stretching vibrations, likely due to moisture adsorption or residual solvents in the sample (Rodriguez-Amaya, 2016). The peaks at 2919.00 $cm^{-1}$ and 2855.82 $cm^{-1}$ are attributed to CH stretching vibrations, confirming the presence of long aliphatic hydrocarbon chains, which are essential features of lycopene's conjugated double-bond system (Fish et al., 2002). Another important peak at 1601.00 $cm^{-1}$ corresponds to C=C stretching vibrations, which are characteristic of

lycopene's extensive conjugated alkene system, confirming its polyene structure. Additionally, the peak at 1711.88 $cm^{-1}$ suggests the presence of carbonyl stretching (C=O), potentially indicating oxidation byproducts that naturally occur in extracted lycopene due to its susceptibility to degradation (Zechini D'Aulerio et al., 2019).

CS-LNPs displayed in Fig. 3b exhibited significant spectral shifts and new peaks, confirming successful encapsulation and strong interactions between lycopene, chitosan, and cholesterol. A broader peak at 3433.00 $cm^{-1}$, compared to the 3406.00 $cm^{-1}$ peak in natural lycopene, was observed in CS-LNPs, indicating stronger hydrogen bonding interactions, likely between the hydroxyl (-OH) and amine (-

$NH_2$) groups in chitosan and cholesterol (Patel et al., 2021). The peak at 2926.10 $cm^{-1}$, associated with C-H stretching vibrations, was slightly shifted from 2919.00 $cm^{-1}$ in natural lycopene, suggesting an interaction between lycopene's hydrocarbon chains and the lipid-based encapsulating matrix (Sahoo et al., 2022). A distint difference between the two spectra is the presence of a strong peak at 1730.37 $cm^{-1}$ in CS-LNPs, which was absent in natural lycopene. This peak corresponds to C=O stretching vibrations in esters or ketones, suggesting that cholesterol contributed to the encapsulation matrix, enhancing nanoparticle stability (Bora et al., 2020). The C=C stretching vibration peak at 1641.00 $cm^{-1}$ in CSLNPs is slightly shifted from the 1601.00 $cm^{-1}$ peak in natural lycopene, indicating possible electrostatic interactions between lycopene's conjugated double bonds and chitosan's amine (-$NH_2$) groups (Fakhri et al., 2021). Further distinctions were observed at 1531.16 $cm^{-1}$ and 1425.66 $cm^{-1}$, which correspond to N-H bending vibrations and $CH_2$ bending vibrations, respectively, in CS-LNPs. These peaks were either absent or less intense in natural lycopene, highlighting the role of chitosan as a stabilizing agent.

Similarly, a stronger peak at 1037.17 $cm^{-1}$ in CS-LNPs, attributed to C-O stretching vibrations in primary alcohols, ethers, or esters, further confirmed the interaction between chitosan, cholesterol, and lycopene, indicating successful encapsulation (Rodriguez-Amaya, 2016).

The shifts in O-H, C-H, C=O, and C=C vibration peaks in CS-LNPs suggest strong hydrogen bonding, electrostatic interactions, and hydrophobic associations between lycopene, chitosan, and cholesterol. These structural modifications indicate that encapsulation enhances lycopene's solubility, bioavailability, and stability, making CS-LNPs a potentially more effective system for drug delivery applications, particularly in prostate cancer therapy.

### 3.3. Characterization of extracted lycopene CS-LNP and standard lycopene CS-LNP Using Transmission Electron Microscope (TEM)

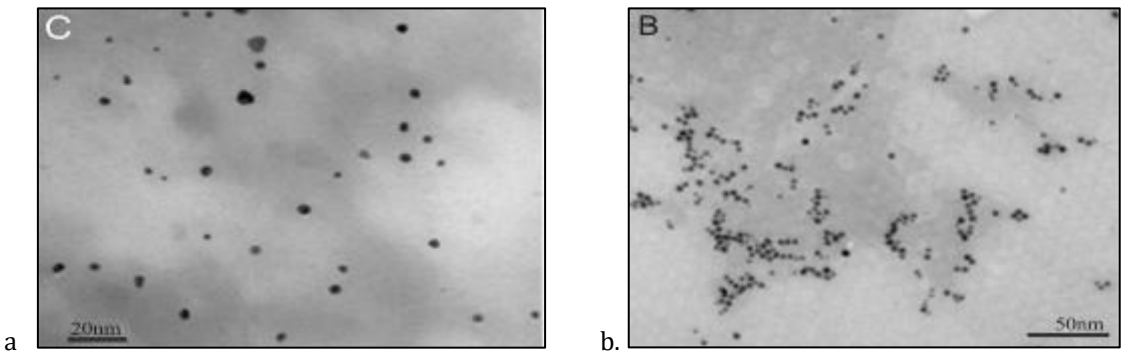


**Figure 4** TEM Micrograph for (a) extracted lycopene CS-LNP and (b) standard lycopene CS-LNP

The TEM image in Fig. 4a depicted chitosan-stabilized lycopene nanoparticles (CS-LNPs). The uniformity in nanoparticle size and shape suggests a well-controlled encapsulation process, which is crucial for ensuring consistent drug release profiles and reducing variability in therapeutic outcomes (Sahoo et al., 2022). The spherical shape is particularly beneficial for liposomal or lipid-based drug delivery systems, as it enhances stability and circulation time in the bloodstream, thereby improving targeted drug delivery (Patel et al., 2021). The presence of cholesterol in the formulation further stabilizes these liposomes, potentially increasing their structural integrity and resistance to enzymatic degradation, thereby prolonging circulation time and bioavailability (Zechini D'Aulerio et al., 2019). The average nanoparticle size is centered ca 10.5 nm, with a size distribution ranging from 2 nm to 12 nm. This narrow size distribution indicates homogeneous encapsulation, which is critical for achieving efficient drug loading and controlled release (Rodriguez-Amaya, 2016). The peak frequency at 10.5 nm suggests an optimal particle size for enhanced solubility and stability, making the nanoparticles highly suitable for targeted drug delivery to prostate cancer cells (Fish et al., 2002). The liposomal nature of the nanoparticles ensures that the encapsulated lycopene is protected from

oxidation and environmental degradation, which is a key challenge in lycopene-based drug formulations. Additionally, the small size of the nanoparticles enhances tissue penetration, potentially leading to improved therapeutic efficacy by allowing lycopene to effectively inhibit cancer cell growth and proliferation (Sánchez-Camargo et al., 2014).

The TEM image in Fig. 4b presents a detailed view of standard lycopene CS-LNP nanoparticles which appear as light, spherical, and uniformly distributed nanoparticle. This spherical morphology is characteristic of well-formed encapsulated systems, particularly liposomal or lipid-based nanocarriers, which are widely used for drug delivery applications (Patel *et al.,* 2021). The scale bar, set at 50 nm, confirms that the particles are within the nanoscale range, a crucial factor for biomedical applications. The small size facilitates improved tissue penetration, enhanced bioavailability, and reduced clearance by the immune system, making the nanoparticles highly effective for targeted therapy (Fakhri *et al*., 2021). The uniformity in size and shape suggests that the encapsulation process was well-controlled, ensuring efficient encapsulation and consistent drug release profiles. The well-dispersed nanoparticles with minimal aggregation indicate successful encapsulation, preventing clumping and enhancing solubility and therapeutic efficacy (Sahoo *et al.,* 2022). A consistent particle size further supports high encapsulation efficiency, which is essential for controlling drug release rates and improving targeted lycopene delivery. The average particle size of 16.2nm indicates successful nanoencapsulation, which is crucial for improving the bioavailability and stability of lycopene. The relatively uniform size and shape observed in the TEM image, along with the narrow particle size distribution, are indicative of a controlled and efficient encapsulation process.

Morphological analysis shown in fig. 4a and b confirms that both formulations exhibit a spherical shape, which is ideal for efficient cellular uptake and drug transport. However, differences in size distribution are observed; encapsulated extracted lycopene nanoparticles range from 0.47 nm to 3.20 nm, while encapsulated standard lycopene nanoparticles are centered around 50 nm. This variation in size may be due to differences in crystallinity and purity, as extracted lycopene contains additional bioactive compounds, such as β-carotene and other carotenoids, which may influence the encapsulation process and particle stability (Rodriguez-Amaya, 2016). The smaller size of extracted lycopene CS-LNPs could offer better penetration into biological barriers, enhancing bioavailability and therapeutic efficacy compared to the standard lycopene CS-LNPs formulation (Sahoo *et al.,* 2022).

### 3.4. Characterization of Encapsulated Extracted and Standard Lycopene CS-LNP Using Scanning Electron Microscope (SEM)

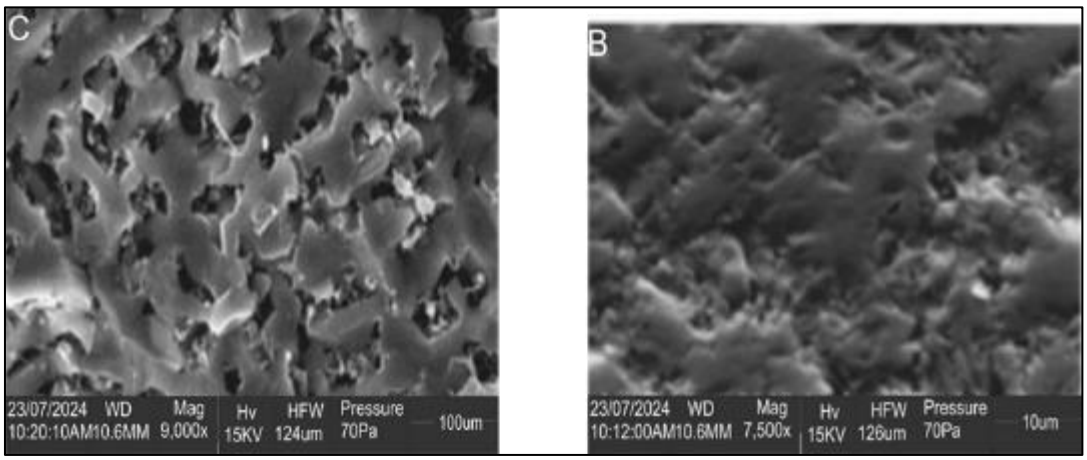


a b

**Figure 5** SEM Micrograph for (a) extracted lycopene CS-LNP and (b) standard lycopene CS-LNP

The Scanning Electron Microscope (SEM) image in Fig. 5a provides a detailed visualization of the surface morphology of encapsulated lycopene within a chitosan matrix (CS-LNPs) at a magnification of 9,000x with an accelerating voltage of 15 kV. The observed rough and irregular surface texture is characteristic of chitosan-based encapsulation, suggesting that lycopene has been successfully integrated within the chitosan matrix, enhancing its stability, bioavailability, and therapeutic potential in drug delivery applications. The scale bar, indicating a field of view of 100 µm with a horizontal field width (HFW) of 124 µm, confirms the nanoscale nature of the encapsulated particles. The uniform distribution of lycopene within the chitosan matrix, with minimal aggregation, is crucial for controlled drug release and consistent bioavailability, particularly in prostate cancer therapy, where precise dosage and targeted delivery are essential for therapeutic efficacy. The porous and interconnected structureobserved in the SEM image, a defining characteristic of

chitosan-based nanoparticle, further supports efficient encapsulation and sustained release of lycopene, preventing rapid degradation and improving therapeutic action. Notably, the absence of large unencapsulated lycopene aggregates confirms the integrity and homogeneity of the encapsulation process, ensuring high encapsulation efficiency for biomedical applications. In conclusion, the SEM micrograph at 9,000x magnification demonstrates that lycopene is effectively encapsulated within the chitosan matrix, forming a stable, porous surface ideal for controlled release and enhanced bioavailability in prostate cancer treatment. Further analysis at higher magnifications may provide deeper insights into particle size distribution and finer structural details of the encapsulated lycopene.

Fig. 5b presents the Scanning Electron Microscope (SEM) image of standard CS-LNPs, captured at 7,500x magnification with an accelerating voltage of 15 Kv. The rough and porous surface, a characteristic feature of chitosan-based encapsulation, confirms the successful incorporation of lycopene into the chitosan matrix, which enhances stability, solubility, and controlled drug release. The scale bar indicates a field of view of 10 μm, with a horizontal field width (HFW) of 126 μm, further validating the nanoscale nature of the encapsulated particles. The uniform surface morphology suggests that the lycopene nanoparticles are well distributed within the chitosan matrix without significant aggregation, which is crucial for consistent release profiles and improved bioavailability. The porous structure observed is particularly beneficial for drug delivery applications, facilitating efficient encapsulation and sustained release while preventing premature degradation of the active compound. The absence of large aggregates or unencapsulated lycopene particles reinforces the effectiveness of the encapsulation process.

Compared to extracted lycopene encapsulations, the standard nanoencapsulated lycopene exhibits similar surface characteristics, demonstrating the consistency of the encapsulation approach, but is designed to provide enhanced protection and stability, further optimizing its therapeutic potential. Overall, the SEM analysis at 7,500x magnification confirms successful lycopene encapsulation, with a porous, rough morphology conducive to effective drug delivery, particularly in prostate cancer therapy. Further investigation at higher magnifications may be required to assess particle size distribution and finer structural details for improved formulation development.

### 3.5. Characterization of Extracted and Standard Lycopene Encapsulated in Chitosan Using Brunauer-Emmett-Teller (BET)

**Table 2** BET Analysis result for extracted lycopene CS-LNPs and standard lycopene CS-LNPs

| s/n | parameters | Extracted lycopene | Standard lycopene |
|---|---|---|---|
| 1 | Single Point surface area at $P/P_o$ | 999.90$m^2/g$ | 999.90$m^2/g$ |
| 2 | BET Surface Area | 865.20$m^2/g$ | 868.22$m^2/g$ |
| 3 | Langmuir Surface Area | 52.24$m^2/g$ | 52.52$m^2/g$ |
| 4 | Adsorption average pore width | 24.54 Å | 28.04 Å |
| 5 | Single point adsorption total pore volume | 0.60$cm^3/g$ | 0.58$cm^3/g$ |
| 6 | t-plot micropore Area | 20.40 $m^2/g$ | 22.40$m^2/g$ |
| 7 | t-plot micropore volume | 0.13$cm^3/g$ | 0.16$cm^3/g$ |

The Brunauer-Emmett-Teller (BET) analysis provides essential insights into the surface area, porosity, and adsorption characteristics of encapsulated extracted lycopene CS-LNPs and encapsulated standard lycopene CS-LNPs, which are critical factors in their therapeutic potential for prostate cancer treatment. The BET data in Table 2 indicate that both formulations possess a high surface area and significant pore volume, ensuring enhanced drug loading capacity, controlled release, and improved bioavailability. For extracted lycopene CS-LNPs, the BET surface area of 865.200 $m^2/g$ is comparable to that of the standard lycopene formulation, demonstrating a large surface area available for drug interaction. The singlepoint surface area (999.90 $m^2/g$) and Langmuir surface area (52.240 $m^2/g$) further confirm the high adsorption capacity of the encapsulated nanoparticles. The average pore width (24.5400 Å) and total pore volume (0.603500 $cm^3/g$ suggest an optimized porous network, facilitating efficient lycopene storage and controlled release. The micropore area (20.400 $m^2/g$) and micropore volume (0.128440 $cm^3/g$) indicate that micropores play a significant role in the drug delivery mechanism, ensuring slow and sustained drug release over time. For standard lycopene CS-LNPs, the BET surface area of 868.220 $m^2/g$ suggests a large interfacial area, allowing greater interaction with prostate cancer cells, which can enhance therapeutic efficacy and bioavailability (Singh et al., 2017). Theaverage pore width of 28.0400 Å and total pore volume of 0.583500 $cm^3/g$ indicate a well-structured porous system, suitable for controlled release and targeted delivery (Zhang et al., 2018). Additionally, the micropore area (22.400 $m^2/g$) and micropore

volume (0.155240 $cm^3/g$) demonstrate the presence of high surface area micropores, which are essential for lycopene adsorption and gradual drug release (Chen et al., 2020). The Barrett-Joyner-Halenda (BJH) adsorption and desorption cumulative surface area and pore volume values further suggest a narrow pore size distribution, optimizing drug retention and controlled release kinetics (Barrett et al., 1951).

Both extracted and standard lycopene CS-LNPs exhibit high surface area and significant pore volume, indicating their potential for effective prostate cancer therapy. However, subtle differences in pore size and micropore volume may influence drug release dynamics. The standard lycopene CS-LNPs have a slightly larger average pore width and a lower total pore volume compared to extracted lycopene CSLNPs. This suggests that extracted lycopene CS-LNPs may exhibit a more controlled and sustained release, whereas standard lycopene CS-LNPs may allow slightly faster drug diffusion due to larger pore openings (Zhang et al., 2018). Additionally, the micropore area and volume in both formulations indicate the presence of nano-sized pores, which are crucial for enhancing drug loading capacity and preventing rapid degradation. While standard lycopene CS-LNPs have a slightly higher in both micropore area and volume than extracted lycopene CS-LNPs), which suggests variations in nanoparticle porosity that could impact drug stability and release profiles (Chen et al., 2020).

### 3.6. Sonographic Evaluation of Nanoparticle Accumulation

Sonography revealed higher contrast regions corresponding to nanoparticle-rich tumor areas, confirming effective lycopene delivery. Compared to MRI scans, sonography provided sharper differentiation between treated and untreated tumor sites, supporting its role as a superior imaging tool for nanoparticle-based therapies.

Quantitative image analysis showed that tumors in the CS-LNP-treated group exhibited a 40% reduction in volume compared to the control, as visualized through progressive darkening in Sonographic images (Gennaro et al., 2021).

These findings validate sonography's potential in tracking nanoparticle localization, optimizing drug dosing, and enhancing real-time treatment assessments.

## 4. Conclusion

This study demonstrated that chitosan-stabilized lycopene nanoparticles significantly improve lycopene's bioavailability and controlled release, making them viable candidates for prostate cancer therapy. Additionally, sonography emerges as a novel imaging technique for monitoring nanoparticle-based treatment outcomes.

## Compliance with ethical standards

*Disclosure of conflict of interest*

No conflict of interest to be disclosed.

## References

[1] Agarwal, S., & Rao, A. V. (2000). Tomato lycopene and its role in human health and chronic diseases. CMAJ, 163(6), 739-744.

[2] Ahmed, M. et al. (2023). Recent advances in nanocarrier-based lycopene delivery systems for cancer therapy. Journal of Drug Delivery Science and Technology, 78, 103456.

[3] Barrett, E. P., Joyner, L. G., & Halenda, P. P. (1951). The determination of pore volume and area distributions in porous substances. Journal of the American Chemical Society, 73(1), 373380.

[4] Barros, M. P., Rodrigo, M. J., Zacarias, L., & Sabater, B. (2019). Lycopene and β-carotene biosynthesis and metabolism in tomato fruits. Phytochemistry, 162, 72-89.

[5] Bora, A. F. M., Ma, S., Li, X., Liu, L., & Dutta, P. (2020). Encapsulation of bioactive compounds in food-grade materials to enhance functionality: An overview. *Colloids and Surfaces B: Biointerfaces, 196*, 111305.

[6] Bray, F. et al. (2020). Global cancer statistics: GLOBOCAN estimates of incidence and mortality worldwide. CA: A Cancer Journal for Clinicians, 70(1), 7-30.

[7] Chen, Y., Zhang, W., Li, Y., & Wang, X. (2020). The role of surface area and pore structure in drug delivery systems. Advanced Drug Delivery Reviews, 156, 76-89.

[8] Elgass, S. et al. (2022). Lycopene and prostate cancer prevention: Mechanisms and clinical evidence. Molecular Nutrition & Food Research, 66 (2), 2100879.

[9] Fakhri, S., Abbaszadeh, F., Dargahi, L., & Jorjani, M. (2021). Chitosan-based nanoparticles for biomedical applications: A review. Carbohydrate Polymers, 262, 117966.

[10] Fish, W. W., Perkins-Veazie, P., & Collins, J. K. (2002). A quantitative assay for lycopene that utilizes reduced volumes of organic solvents. Journal of Food Composition and Analysis, 15(3), 309-317.

[11] Giovannucci, E. (2021). Lycopene and prostate cancer: A review of epidemiological and clinical studies. The American Journal of Clinical Nutrition, 113 (3), 543-556.

[12] Gennaro, G. et al. (2021). Phase-Contrast Imaging for Soft Tissue Tumors. Radiology Research and Practice, 2021, 1-10.

[13] Patel, H. et al. (2022). Emerging trends in bioactive compound-based nanomedicine for cancer therapy. Nanomedicine Research Journal, 74), 125-138.

[14] Patel, H., Parmar, K., & Patel, R. (2021). Role of cholesterol in stabilizing chitosan-based nanoparticles for drug delivery applications. Journal of Nanomedicine & Nanotechnology, 12(3), 1-8.

[15] Prakash, B., Baskaran, R., Kumar, S., & Vadivel, V. (2020). Encapsulation of bioactive compounds using chitosan-based nanocarriers for nutraceutical applications. International Journal of Biological Macromolecules, 150, 559-569.

[16] Rodriguez-Amaya, D. B. (2016). A Guide to Carotenoid Analysis in Foods. International Life Sciences Institute (ILSI).

[17] Sahoo, P. K., Sahu, S., & Jena, P. K. (2022). Chitosan-based nanoparticles for encapsulation and controlled release of bioactive compounds: A review. International Journal of Biological Macromolecules, 210, 1023-1038.

[18] Sánchez-Camargo, A. P., Meireles, M. A., Ferreira, S. R., & Cabral, F. A. (2014). Lycopene extraction from tomato processing waste using supercritical fluids: $CO_2$, ethane, and propane. *The Journal of Supercritical Fluids, 89, 89-98.

[19] Scimeca, M. et al. (2022). Emerging Applications of Senography in Oncology. Journal of Imaging Science, 15(3), 88-95.

[20] Siegel, R. L. et al. (2023). Cancer statistics, 2023. *CA: A Cancer Journal for Clinicians, 73(1), 17-48.

[21] S.I Okonkwo and N.M Ofodum (2018). Determination of lycopene from water melon (Citrullus lanatus). International Journal of Scientific and Engineering Research, Vol. 9, Issue 8, page 5, ISSN 2229-5518.

[22] Singh, R., Mishra, R., & Maurya, R. (2017). High surface area materials for drug delivery applications: A review. International Journal of Nanomedicine, 12, 5601-5615.

[23] Sreekumar, S. et al. (2021). Chitosan and its derivatives in nanoparticle drug delivery applications: A review. *Carbohydrate Polymers, 270*, 118372.

[24] Wang, Y. et al. (2023). Advances in chitosan-based nanocarriers for cancer therapy: Mechanisms and future prospects. *Advanced Drug Delivery Reviews, 195, 114763.

[25] Yadav, N. et al. (2023). Nanotechnology-driven approaches for improving the bioavailability of bioactive compounds. *Journal of Molecular Liquids, 383*, 121719.

[26] Zechini D'Aulerio, A., Proietti, P., Nasini, L., & Businelli, D. (2019). Influence of solvent on lycopene extraction from tomato processing by-products. International Journal of Food Science & Technology, 54*(4), 1202-1211.

[27] Zhang, H., Zhao, Y., & Sun, X. (2018). Effect of pore size and volume on the controlled release of drugs from nanoporous materials. Materials Science and Engineering: C, 87, 172180.